Mixed Spectral Element Method for Electromagnetic Secondary Fields in Stratified Inhomogeneous Anisotropic Media

TINGTING HUANG[1,2], MINGWEI ZHUANG[1,2], JIANLIANG ZHUO[1,2], RONGHAN HONG[1,2], YUEFENG SUN[3], AND QING HUO LIU[4], (Fellow, IEEE)

[1]Institute of Electromagnetics and Acoustics, Xiamen University, Xiamen 361005, China
[2]Fujian Provincial Key Laboratory of Electromagnetic Wave Science and Detection Technology, Xiamen University, Xiamen 361005, China
[3]Department of Geology and Geophysics, Texas A&M University, College Station, TX 77843, USA
[4]Department of Electrical and Computer Engineering, Duke University, Durham, NC 27708, USA

Corresponding authors: Mingwei Zhuang (mw.zhuang@xmu.edu.cn) and Qing Huo Liu (qhliu@duke.edu)

ABSTRACT The spectral element method (SEM) is widely used for analyzing high frequency electromagnetic wave propagation and scattering in complex structures. At low frequencies, however, the primary (direct) fields are usually much larger than the secondary fields caused by scattering, thus making it much more difficult to accurately simulate the secondary (scattered) fields because of the source singularity in the primary fields. To more effectively and accurately simulate the low-frequency secondary fields in subsurface structures, in this work the vector Helmholtz equation for the scattered fields is used to directly obtain the secondary field data in inhomogeneous anisotropic media. The computational method for the secondary electromagnetic fields is based on the mixed spectral element method (mixed SEM) for anisotropic objects in a layered anisotropic background medium. The electromagnetic field is separated into the background fields that are evaluated analytically using the dyadic Green's functions (DGFs) of a layered uniaxially anisotropic medium, and the secondary fields caused by anomalous bodies with arbitrary shapes are numerically computed by the mixed SEM. This avoids the source singularity, and allows the transmitters to be located outside the computational domain. By enforcing Gauss' law as the constraint condition, the mixed SEM efficiently eliminates the low frequency breakdown problem. Numerical results verify the proposed method over the traditional SEM in low-frequency scattering from objects in subsurface layered anisotropic media.

INDEX TERMS Mixed spectral element method, secondary field, anisotropic media, source singularity.

I. INTRODUCTION

In modelling the responses of electromagnetic (EM) surveys for geophysical exploration, it is usually necessary to separate the EM fields into the primary (background) field in the subsurface background (i.e., the subsurface without the specific scatterers) and the secondary(scattered) field due to the responses of the specific scatterers (i.e., anomalies) in the subsurface background. The secondary fields are widely employed in various EM exploration methods such as multi-component induction tools [1], controlled-source electromagnetic (CSEM)

method [2], the marine controlled-source electromagnetic (MCSEM) method [3], inversion of airborne electromagnetic data [4], helicopter-borne electromagnetic (HEM) measurements [5], semi-airborne electromagnetic method (SAEM) [6], the ground-airborne frequency-domain electromagnetic (GAFDEM) survey [7], ground penetrating radar [8], [9] and other detection methods [10], [11].

To compute the secondary field numerically, various techniques such as the finite difference method (FDM), the finite element method (FEM), and the spectral element method (SEM) have been developed. Newman *et al.* obtained the 3-D airborne EM responses of secondary field by using FDM in frequency-domain [12]. Liu *et al.* established a 2-D time-domain transient electromagnetic response of the line

The associate editor coordinating the review of this manuscript and approving it for publication was Xiaokang Yin.

source in the FDM [13]. They showed that the secondary field simulation method is faster and more accurate than the total field simulation method because of the removal of the primary field near the source. Recently, Hu *et al.* derive a generalized formulation of the finite difference time domain method for the simulation model with uniaxial anisotropy using a perfectly matched layer as absorbing boundary conditions [14]. However, the FDM adopts a structured grid, which may cause a large geometric error when modelling realistic and complex curved structures. The FEM is preferred in subsurface exploration for its flexibility in modelling more realistic and complex topography. Li *et al.* developed a 2.5-D frequency-domain airborne EM algorithm for forward modelling and inversion, and the secondary fields are solved by the FEM [4]. For the multicomponent induction logging tool in electromagnetic well logging problems, Sun and Nie employed the hierarchical mixed order vector FEM to improve the numerical accuracy and computational efficiency of secondary fields [1]. Grayver *et al.* presented a robust and scalable secondary field solver based on the adaptive mesh FEM; it was applied to large-scale 3-D geo-electromagnetic forward modelling problems with a linear system having 200 million unknowns are solved [15]. The linear edge-based finite element method was applied to solve the diffusive electromagnetic problem in an anisotropic conductive medium [2], and anomalous bodies can be discretized using rectangular hexahedron elements. As is well known, traditional numerical methods in subsurface electromagnetic exploration often suffer from the low frequency breakdown problem due to their use of vector Helmholtz equation without the constraint of Gauss' law [16]–[18]. Physically, this is because the electric and magnetic fields are increasingly decoupled as the frequency decreases, and the EM field is dominated by Gauss' law and Faraday's law, thus leading to low frequency breakdown phenomenon in solving the pure vector Helmholtz equation directly if Gauss' law is not fully accounted for. Recently, the mixed FEM technique, by imposing the Gauss' law as a constraint condition in the secondary field governing equations, is used for modelling the bioelectromagnetism model from direct current (DC) to microwave frequencies [18]. One of the advantages of the mixed FEM is its ability to overcome the numerical breakdown problem and improve the accuracy in the low frequency regime. However, in the above methods, the primary fields are either calculated analytically in an isotropic layered model or a homogeneous anisotropic model.

Different from the above previous works, the new contribution of this work is to use the mixed SEM to solve secondary fields with a layered anisotropic background medium. The field singularity near the imposed sources can be avoided based on the vector Helmholtz equation for the scattered field, and the secondary fields are solved by using the mixed SEM. By exploiting the Gauss' law as the constraint condition in the mixed SEM, the low frequency breakdown problem be eliminated. In addition, the primary fields are evaluated analytically using the dyadic Green's functions (DGFs) for a

layered anisotropic medium, while the equivalent sources in anomalous bodies can be solved easily. Meanwhile, the transmitters can be outside the computational domain, which greatly reduces the computational domain and increases the efficiency. Most importantly, both the scatterers and the background medium can have electric and magnetic anisotropy. Compared with FEM, the high-order polynomial basis functions in the mixed SEM achieve exponential convergence with the order of polynomial basis functions, and improve the accuracy and efficiency in the computation of secondary fields.

The remainder of the paper is arranged as follows. In Section II, we briefly introduce the secondary field based mixed SEM and DGFs for a uniaxially anisotropic layered background medium. In Section III, the implementation of our method in scattering analysis of biaxial anisotropic objects embedded in a layered uniaxial anisotropic medium is presented. Finally, the conclusion is drawn in Section IV.

II. THEORY

In a typical secondary field problem of subsurface EM simulation, the anomalous bodies are present in a layered earth with anisotropic medium with relative complex permittivity $\overline{\overline{\epsilon}}_{rb}$ and relative complex permeability $\overline{\overline{\mu}}_{rb}$. The anomalous bodies have complex geometrical shapes with arbitrary anisotropy. The combination of the mixed SEM and dyadic Green's functions is applied to solving the secondary field. The time dependence $e^{j\omega t}$ is implied in the following formulations.

A. MIXED SEM THEORY

For the 3-D low-frequency secondary field problem in an inhomogeneous anisotropic medium, the scattered magnetic field $\mathbf{H}^s$ is governed by the vector Helmholtz equation and the Gauss' law,

$$\nabla \times (\overline{\overline{\epsilon}}_r^{-1} \nabla \times \mathbf{H}^s) - k_0^2 \overline{\overline{\mu}}_r \mathbf{H}^s$$
$$= j\omega\varepsilon_0 \nabla \times (\mathbf{I} - \overline{\overline{\epsilon}}_{rb}\overline{\overline{\epsilon}}_r^{-1})\mathbf{E}^i + k_0^2(\overline{\overline{\mu}}_r - \overline{\overline{\mu}}_{rb})\mathbf{H}^i$$

(1)

$$\nabla \cdot (\overline{\overline{\mu}}_r \mathbf{H}^s) = \nabla \cdot \left[(\overline{\overline{\mu}}_{rb} - \overline{\overline{\mu}}_r)\mathbf{H}^i\right]$$

(2)

where k_0 and ε_0 are the wavenumber and permittivity in vacuum, ω is the angular frequency, $\mathbf{I}$ is the unit tensor, and $\overline{\overline{\epsilon}}_r$ and $\overline{\overline{\mu}}_r$ are the relative complex permittivity and permeability in the model, respectively. Note that the subscript b denotes the background. The source terms involve the incident electric field $\mathbf{E}^i$ and magnetic field $\mathbf{H}^i$ in the layered anisotropic background medium, which can be computed by the DGFs of the vector potentials in an unbounded anisotropic medium [19]. Note that the secondary fields, unlike the primary fields, are not singular near transmitter locations because the scattered field equations have removed the excitation source terms in the conventional total-field equation. The scattered electric field $\mathbf{E}^s$, similarly, can be obtained simply by the duality theorem.

In order to simulate the scattered field responses to complex geological structures using the mixed SEM in an unbounded medium, the perfectly matched layer (PML) surrounded by a perfect magnetic conductor (PMC) is used as an absorbing boundary condition. The weak form of the vector Helmholtz equation and Gauss' law for the scattered field is to seek $\mathbf{H}^s \in \mathbf{H}$ (curl, Ω), such that

$$(\nabla \times \mathbf{w}, \overline{\overline{\varepsilon}}_r^{-1} \nabla \times \mathbf{H}^s)_\Omega - k_0^2(\mathbf{w}, \overline{\overline{\mu}}_r \mathbf{H}^s)_\Omega$$
$$= j\omega\varepsilon_0(\nabla \times \mathbf{w}, (\mathbf{I} - \overline{\overline{\varepsilon}}_{rb}\overline{\overline{\varepsilon}}_r^{-1})\mathbf{E}^i)_\Omega + k_0^2(\mathbf{w}, (\overline{\overline{\mu}}_r - \overline{\overline{\mu}}_{rb})\mathbf{H}^i)_\Omega$$
$$\forall \mathbf{w} \in \mathbf{H}(\text{curl}, \ \Omega) \qquad (3)$$

$$(\nabla q, \overline{\overline{\mu}}_r \mathbf{H}^s)_\Omega$$
$$= (\nabla q, (\overline{\overline{\mu}}_{rb} - \overline{\overline{\mu}}_r)\mathbf{H}^i)_\Omega, \forall q \in H^1(\Omega) \qquad (4)$$

where the first term of Eq. (3) produces the singular stiffness matrix; its second term produces the well-conditioned mass matrix, while the right hand side is the equivalent sources. However, in subsurface EM exploration, a low-frequency electrical current is usually used as a source to excite electromagnetic fields. The stiffness matrix plays a dominant role in the low-frequency system as the mass-matrix term diminishes because it is proportional to the square of frequency; the dominant singular stiffness matrix causes the system matrix to become singular, thus introducing the well-known low-frequency breakdown problem. Hence, it is difficult to obtain an accurate solution with an iterative solver or direct solver due to the ill-conditioned system matrix in the low-frequency regime.

To overcome the low frequency breakdown problem, the mixed SEM is used by imposing Eq. (4) as the divergence constraint condition to suppress the effect of the singularity of Eq. (3), hence the property of the system matrix is significantly improved. A detailed proof of the mixed SEM or mixed FEM to overcome the low-frequency breakdown by introducing the divergence constraint condition and achieves fast convergence solutions was given in References [16], [17]. Then, Eq. (4) is imposed into Eq. (3) by the Lagrange multiplier $p \in H^1(\Omega)$, leading to the weak formulation of the mixed SEM

$$(\nabla \times \mathbf{w}, \overline{\overline{\varepsilon}}_r^{-1} \nabla \times \mathbf{H}^s)_\Omega - k_0^2(\mathbf{w}, \overline{\overline{\mu}}_r \mathbf{H}^s)_\Omega + \alpha k_0^2(\overline{\overline{\mu}}_r \mathbf{w}, \nabla p)_\Omega$$
$$= j\omega\varepsilon_0(\nabla \times \mathbf{w}, (\mathbf{I} - \overline{\overline{\varepsilon}}_{rb}\overline{\overline{\varepsilon}}_r^{-1})\mathbf{E}^i)_\Omega + k_0^2(\mathbf{w}, (\overline{\overline{\mu}}_r - \overline{\overline{\mu}}_{rb})\mathbf{H}^i)_\Omega$$
$$\forall \mathbf{w} \in \mathbf{H}(\text{curl}, \Omega) \qquad (5)$$

$$\alpha(\nabla q, \overline{\overline{\mu}}_r \mathbf{H}^s)_\Omega$$
$$= \alpha(\nabla q, (\overline{\overline{\mu}}_{rb} - \overline{\overline{\mu}}_r)\mathbf{H}^i)_\Omega, \forall q \in H^1(\Omega) \qquad (6)$$

where α is a scaling constant to balance the Gauss' law with the vector Helmholtz equation. In this way, we can obtain accurate solutions even when the frequency is extremely low.

In the mixed SEM, the curl-conforming vector basis functions Φ_n are used to expand the scattered magnetic field $\mathbf{H}^s$ to achieve exponential convergence (i.e., the error decreases exponentially with the order of basis functions), and the nodal basis functions are employed to expand the scalar function p. Employing the Galerkin's method, a discrete linear system

can be obtained as follows

$$\begin{pmatrix} \mathbf{S} - k_0^2\mathbf{M} & \mathbf{K} \\ \mathbf{K}^T & 0 \end{pmatrix} \begin{pmatrix} \mathbf{x} \\ \mathbf{y} \end{pmatrix} = \begin{pmatrix} \mathbf{b} \\ \mathbf{c}_a \end{pmatrix} \qquad (7)$$

where $\mathbf{S}$ is the stiffness matrix, $\mathbf{M}$ is the mass matrix, $\mathbf{K}$ is the constraint matrix, $\mathbf{K}^T$ is the transpose of $\mathbf{K}$; vectors $\mathbf{x}$ and $\mathbf{y}$ denote the unknowns of $\mathbf{H}^s$ and p, respectively; $\mathbf{b}$ and $\mathbf{c}_a$ are the source terms corresponding to the right-hand sides of Eq. (5) and (6). The elements of the above matrices are given follows:

$$\mathbf{S}_{mn} = \int_\Omega (\nabla \times \Phi_m) \cdot (\overline{\overline{\varepsilon}}_r^{-1} \nabla \times \Phi_n) dV$$

$$\mathbf{M}_{mn} = \int_\Omega \Phi_m \cdot \overline{\overline{\mu}}_r \Phi_n dV$$

$$\mathbf{K}_{mn} = \alpha k_0^2 \int_\Omega \overline{\overline{\mu}}_r \Phi_m \cdot \nabla q_n dV$$

$$\mathbf{b}_m = k_0^2 \int_\Omega \Phi_m \cdot (\overline{\overline{\mu}}_r - \overline{\overline{\mu}}_{rb})\mathbf{H}^i dV$$
$$+ j\omega\varepsilon_0 \int_\Omega \nabla \times \Phi_m \cdot (\mathbf{I} - \overline{\overline{\varepsilon}}_{rb}\overline{\overline{\varepsilon}}_r^{-1})\mathbf{E}^i dV$$

$$(\mathbf{c}_a)_m = \alpha k_0^2 \int_\Omega \nabla q_m \cdot (\overline{\overline{\mu}}_{rb} - \overline{\overline{\mu}}_r)\mathbf{H}^i dV \qquad (8)$$

where subscripts m and n denote the indices of testing and basis functions, respectively.

B. DYADIC GREEN's FUNCTIONS IN A LAYERED UNIAXIALLY ANISOTROPIC MEDIUM

By evaluating the dyadic Green's functions of the magnetic vector potential $\mathbf{A}$ (DGFA) and that of the electric vector potential $\mathbf{F}$ (DGFE) for an uniaxially anisotropic multilayered medium and solving for the electric and magnetic flux densities numerically, the background fields $\mathbf{E}^i$ and $\mathbf{H}^i$ can be calculated easily. With Sommerfeld integration, the calculation of DGFA in the uniaxial anisotropic medium is expressed as [20]

$$\overline{\overline{\mathbf{G}}}_{\mathbf{AJ}}(\mathbf{r}, \mathbf{r}') = \frac{1}{(2\pi)^3} \iiint_{-\infty}^{+\infty} \frac{\overline{\overline{Z}}_A^a}{|\overline{\overline{Z}}_A|} e^{-j\mathbf{k}\cdot(\mathbf{r}-\mathbf{r}')} d\mathbf{k} \qquad (9)$$

where $\mathbf{r}$ and $\mathbf{r}'$ denote the receiver position and the source position in Cartesian coordinate system, respectively. $\mathbf{k}$ is the wave vector, $\overline{\overline{Z}}_A$ and $\overline{\overline{Z}}_A^a$ are the electric wave matrix and its adjoint, and $|\overline{\overline{Z}}_A|$ is determinant of $\overline{\overline{Z}}_A$. More detailed derivation can be referred to [20].

Notice that Eq. (9) is utilized to compute the DGFA when $\mathbf{r}$ and $\mathbf{r}'$ are different. When the two position vectors coincide, Eq. (9) cannot be directly used to compute DGFA because of the singularity. The numerical mean value is used to address the problem [20]. Finally, the DGFE can be obtained by the duality theorem.

III. NUMERICAL RESULTS

In this section, two numerical results are demonstrated to verify the performance of the proposed mixed SEM in computing the scattered fields of inhomogeneous anisotropic objects embedded in a layered uniaxial anisotropic background medium, and its effectiveness in removing the source
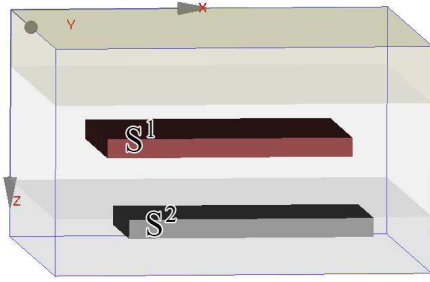
FIGURE 1. Geometry of inhomogeneous isotropic objects with arbitrary shapes embedded in a three-layer background medium.

singularity. Advantages of this method is shown over the traditional total-field solver. The reference solutions are obtained by the total-field solver by subtracting the incident field $\mathbf{H}^i$ from the total field $\mathbf{H}^t$, where the total field results are calculated by the mixed SEM by using the total field-based formulation, and the incident field is obtained analytically through the DGFs. All of the examples are performed on a workstation with 20-cores Xeon E2650 v3 2.3-GHz CPU and 512-GB RAM.

A. TWO SCATTERERS EMBEDDED IN A THREE-LAYER MEDIUM

Two regular scatterers are embedded in a layered background model with the size of 2 km × 2 km × 1.2 km, where the two isotropic objects are located at the middle layer and the bottom layer, respectively, as shown in Fig. 1. The thicknesses of the three layers are 300 m, 600 m and 300 m along the positive z-axis, respectively. The top layer is air. The relative permittivity and conductivity (ϵ_r, σ) are (3, 0.0015) for the middle layer, (2, 0.001) for the bottom layer; (4, 0.002) for scatterer 1, and (5, 0.003) for scatterer 2.

Three electric dipole sources polarized in the direction (1, 1, 0) are located at (0.6, 1.2, 0.325) km, (1.6, 1.2, 0.325) km and (2.6, 1.2, 0.325) km and operate at 50 Hz. Note the third source is outside the computational domain in the scattered field solver, but it must be included in the total field solver. When the sources are far away from the region of interest, however, it is extravagant to enlarge the computational domain to include all sources in the total field solver. In contrast, in the scattered field formulation used here, only the incident fields are needed, so the source can be directly deployed outside the computational domain to efficiently perform regional simulations. The computational domain is discretized using 11,088 elements with 1,157,567 DoFs in the 3th-order mixed SEM by the scattered field formulation. However, in the total field based solver with the same mesh size, a larger computational domain (such as the size expanding to 2.8 km along x-axis) needs to be discretized into 13,860 elements with 1,450,013 (or over 25% more) DoFs to include all sources. Two layers of PML spectral elements in the damping direction are implemented on all the six sides of the model. The receiver array is deployed on the intersection of plane $y = 1.5$ km and plane $z = 250$ m, while the x value
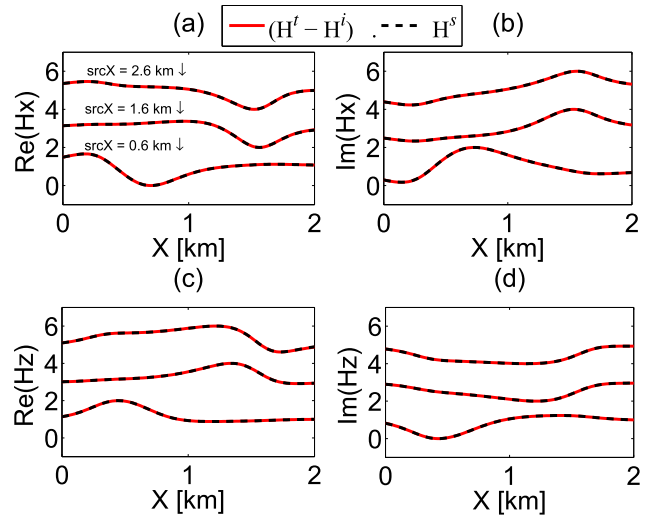
FIGURE 2. Secondary H field components from this scattered field solver along the receiver line in the three-layer medium are compared with the total-field formulation. The real part(a) and imaginary part(b) of the H_x^s component. The real part(c) and imaginary part(d) of the H_z^s component. The scattered field solver needs 1,157,567 DoFs, while the total field solver needs 1,450,013 (or over 25% more) DoFs to include the sources.
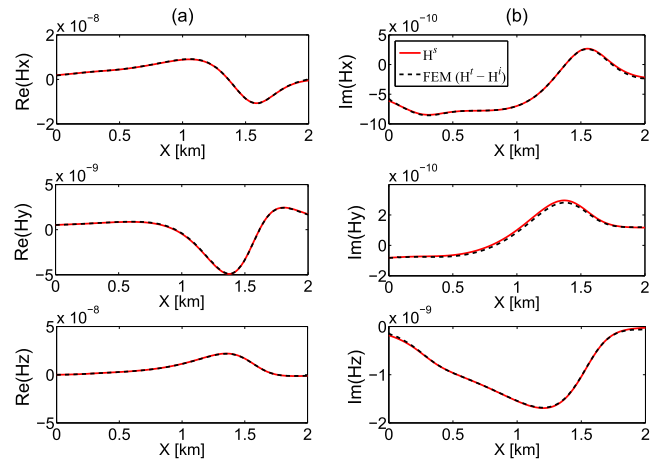

FIGURE 3. Secondary H field components from this scattered field solver along the receiver line in the three-layer medium are compared with the total-field formulation in FEM when the source is at (1.6, 1.2, 0.325) km. The real part(a) and imaginary part(b) of the three components.

is 0 to 2 km with 20 m interval in the air layer. In Fig. 2, all waveforms are normalized individually with respect to the maximum value of the reference results. Our results agree well with the reference solutions from the total field solver, and the relative L_2 norm error is 1.3%. These results show that the scattered field solver developed here is accurate and more efficient than the total field solver, especially when the sources are far way from the region of interest.

To demonstrate the advantage of the mixed SEM in low frequency electromagnetic exploration, we also compared the proposed method with the commercial FEM software (COMSOL Multiphysics). Note that the conductivity of the air layer is 0.0008 S/m because of the FEM solutions fails to converge (low frequency breakdown phenomenon) when
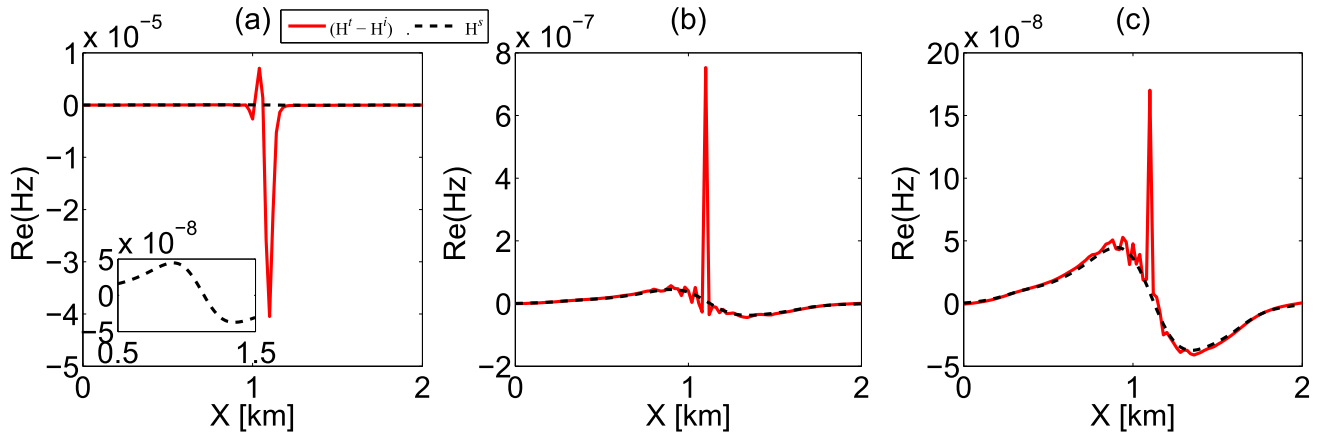
FIGURE 4. Comparison between the scattered field solver (with 11088 elements) and total field solver when the source is near the survey line. The real part of the z component of the scattered field near the source when the receivers are deployed along the x direction with y = 1.23 km and z = 0.325 km. The mesh in the total field solver uses (a) 11088, (b) 26970 and (c) 52022 elements to refine the mesh in the model in Fig. 1, respectively. The total field solver needs nearly 4 times more DoFs than the scattered field solver, and yet the source singularity still has not been completely removed.

$\sigma = 0$ in low frequency problems. The DoFs of FEM is 4,591,659 with the 3rd-order basis functions and the results are shown in Fig. 3. It is shown that excellent agreement is achieved between the mixed SEM results and the FEM solutions with its total field subtracted by the incident field.

Next, we show that the scattered field solver is more efficient when the sources are near the region of interest also, because it can handle the source singularity much better. If the survey line is close to the transmitter, the fields obtained by the total-field solver may be singular and incur a large error. As shown in Fig. 4 (a), when the survey line of receiver is about 30 m away from the transmitter located at (1.1, 1.2, 0.325) km, the secondary field responses are smooth and continuous for our method, while they are singular in the total-field simulation. The singularity, however, can be reduced by refining the mesh around the source location, as shown in Fig. 4 (b) and (c). The singularity with 52,022 elements is almost 3 orders of magnitude smaller than that without mesh refinement, but the singularity still cannot be completely resolved. Meanwhile, mesh refinement around the source location not only increases the difficulty of mesh generation, but also increases the number of unknowns significantly, especially for multi-source problems. As discussed above, the scattered field solver based on the mixed SEM not only simulates the secondary field responses accurately, but also allows multiple sources and sources outside the computational domain. The field singularity near the imposed sources is avoided.

B. INHOMOGENEOUS BIAXIAL ANISOTROPIC SCATTERERS EMBEDDED IN AN EIGHT-LAYER UNIAXIAL ANISOTROPIC MEDIUM

In this example, we simulate a more challenging anticline reservoir structure in an eight-layer model, as shown in Fig. 5. The computational domain is 6 km × 5 km × 4.5 km, and the thickness of those layers along the z-axis from L^1 to L^8 is
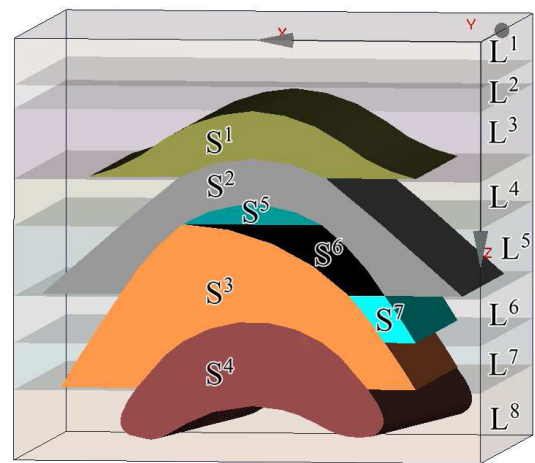
FIGURE 5. Anticline reservoir structure-like model with inhomogeneous biaxial anisotropic objects embedded in an 8-layer uniaxial anisotropic background medium.

385 m, 380 m, 700 m, 350 m, 525 m, 350 m, 350 m and 910 m, respectively. All of the media are anisotropic except for the top air layer, and the material properties of the scatterers and layers are provided in Table 1 [21].

An electric dipole source polarized at (1, 1, 1) and operating at 20 Hz is located at (3, 1.25, 0.4) km. The computational domain is discretized into 80,223 elements with 8,514,548 DoFs in the 3th-order mixed SEM. If a source is far away from the computational domain, such as 15 km in the y direction from the center of the geometry, the total field solver require a model at least three times larger, which will triple the number of DoFs and consume a lot of computing resources. Three layers of PML spectral elements in the damping direction are utilized on all the six sides of the model. At a receiver array along the z direction with x = y = 0.5 km, our results agree well with the reference solutions from the total field solver, as shown in Fig. 6, and the L_2 norm error is 1.2%. This example demonstrates that the proposed

TABLE 1. The EM parameters of fifteen materials of the 3-D model in Fig. 5.

| Scatterer / Layer	Relative Permittivity	Relative Permeability	Conductivity (S/m)
S^1, L^4	diag(3, 3, 2)	1	diag($1.0e^{-3}, 1.0e^{-3}, 2.0e^{-3}$)
S^2, L^6	diag(5.8, 5.8, 8)	1	diag($3.0e^{-4}, 3.0e^{-4}, 4.0e^{-4}$)
S^3, L^8	diag(12, 12, 13)	1	diag($5.3e^{-5}, 5.3e^{-5}, 8.0e^{-5}$)
S^4	diag(9, 10, 11)	diag(12, 10, 13)	$\begin{bmatrix} 2.0e^{-5} & 1.0e^{-5} & 2.0e^{-5} \\ 1.0e^{-5} & 3.0e^{-5} & 1.0e^{-5} \\ 2.0e^{-5} & 1.0e^{-5} & 2.0e^{-5} \end{bmatrix}$
S^5	diag(6.7, 7.2, 7)	diag(7, 9, 7.5)	diag($5.0e^{-4}, 2.0e^{-4}, 1.0e^{-4}$)
S^6	diag(18, 20, 19)	diag(22, 19, 20)	diag($1.2e^{-3}, 1.0e^{-3}, 3.0e^{-3}$)
S^7	81	diag(6, 6.2, 5)	diag($1.0e^{-5}, 6.0e^{-5}, 3.0e^{-5}$)
L^1	1	1	0
L^2	diag(3.6, 3.6, 3)	1	diag($1.2e^{-3}, 1.2e^{-3}, 1.3e^{-3}$)
L^3	diag(4.3, 4.3, 4)	1	diag($1.7e^{-3}, 1.7e^{-3}, 1.9e^{-3}$)
L^5	diag(5.2, 5.2, 5)	1	diag($1.8e^{-3}, 1.8e^{-3}, 1.5e^{-3}$)
L^7	diag(5.8, 5.8, 6)	1	diag($2.3e^{-3}, 2.3e^{-3}, 2.0e^{-3}$)
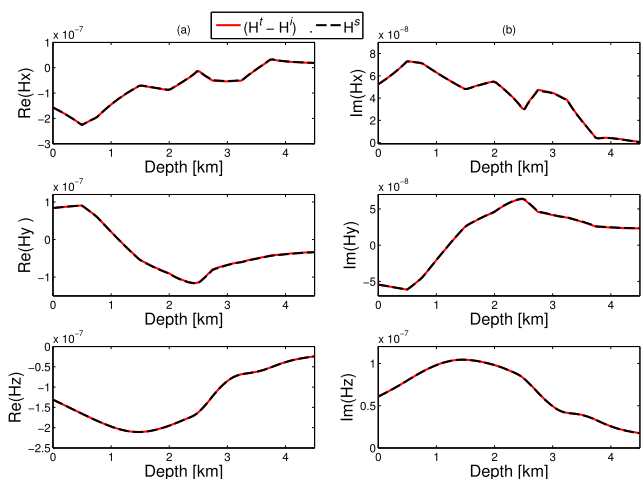
FIGURE 6. Secondary H^s fields along the receiver line in the eight layered medium is compared with those from the total field solver. (a) and (b) are for the real and imaginary parts of the scattered magnetic fields, respectively.

FIGURE 7. Secondary H^s field distribution for the 3-D model in Fig. 5. (a) Field pattern H^s (A/m) on the *xy* plane view with $z = 0.2$ km. (b) Field pattern H^s (A/m) in the *xz* plane view with $y = 2.3$ km.

method is capable of handling scattering analysis of biaxial anisotropic multi-target embedded in a multi-layer uniaxial anisotropic medium with high accuracy compared to the total field formulation.

Now, placing a high power 2 km line source located at the ground parallel to the *y*-direction with the start-point at (3, 0.2, 0.4) km and having current amplitude as 1 A, we present the result at 20 Hz in the form of field distribution. As illustrated in Fig. 7 (a) on a horizontal cross section $z = 0.2$ km in the air, the secondary field induced by the reservoir rocks is clearly visible. Due to the nearby line source, the middle zone is especially obvious. Furthermore, Fig. 7 (b) for the field distribution in the *xz* cross section at $y = 2.3$ km gives a clear perspective of the anomalous bodies in the underground space corresponding to the design in Fig. 5: the extremely strong field can be seen as caused by the source. This analysis
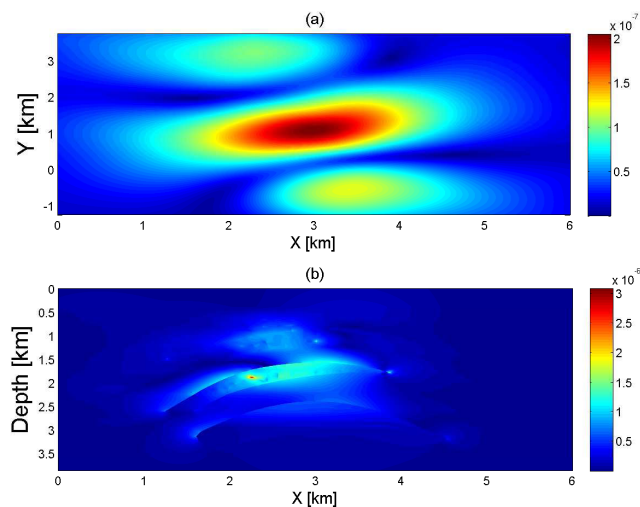
offers a clear scattering effect for the multitargets inverse problem.

IV. CONCLUSION

In this work the scattered field solver based on the vector Helmholtz equation combined with Gauss' law is developed to simulate the secondary field responses in stratified anisotropic media to avoid the source singularity and the low frequency breakdown problem. It allows the transmitters to be located outside the computational domain. The background fields are obtained analytically by evaluating the dyadic Green's functions of layered uniaxial anisotropic media. The major advantage of the mixed SEM is that it can overcome the numerical breakdown problem in low-frequency subsurface EM simulation and improve the numerical accuracy. Numerical results show the accuracy of the proposed method in

solving secondary field responses of subsurface EM simulation with complex 3D geologic structures.

REFERENCES

[1] X. Y. Sun and Z.-P. Nie, "Vector finite element analysis of multicomponent induction response in anisotropic formations," *Prog. Electromagn. Res.*, vol. 81, pp. 21–39, 2008.

[2] H. Cai, B. Xiong, M. Han, and M. Zhdanov, "3D controlled-source electromagnetic modeling in anisotropic medium using edge-based finite element method," *Comput. Geosci.*, vol. 73, pp. 164–176, Dec. 2014.

[3] N. V. da Silva, J. V. Morgan, L. MacGregor, and M. Warner, "A finite element multifrontal method for 3D CSEM modeling in the frequency domain," *Geophysics*, vol. 77, no. 2, pp. 101–115, Mar. 2012.

[4] W.-B. Li, Z.-F. Zeng, J. Li, X. Chen, K. Wang, and Z. Xia, "2.5D forward modeling and inversion of frequency-domain airborne electromagnetic data," *Appl. Geophys.*, vol. 13, no. 1, pp. 37–47, Mar. 2016.

[5] B. Siemon, "Levelling of helicopter-borne frequency-domain electromagnetic data," *J. Appl. Geophys.*, vol. 67, no. 3, pp. 206–218, Mar. 2009.

[6] X. Wu, G. Xue, G. Fang, X. Li, and Y. Ji, "The development and applications of the semi-airborne electromagnetic system in China," *IEEE Access*, vol. 7, pp. 104956–104966, 2019.

[7] C. Liu, L. Kang, W. Zhu, H. Zhou, M. Zhang, and J. Liang, "Suppression of the attitude error with a modified iterative algorithm for apparent resistivity imaging in gafdem survey," *IEEE Access*, vol. 7, pp. 179898–179904, 2019.

[8] H. Liu, C. Lin, J. Cui, L. Fan, X. Xie, and B. F. Spencer, "Automatic detection and localization of rebar in concrete by deep learning using ground penetrating radar," *Automat. Constr.*, vol. 118, no. 10, Oct. 2020, Art. no. 103279.

[9] H. Liu, H. Lu, J. Lin, F. Han, C. Liu, and B. F. Spencer, "Penetration properties of ground penetrating radar waves through rebar grids," *IEEE Trans. Geosci. Remote Sens.*, early access, Jun. 4, 2020, doi: 10.1109/LGRS.2020.2995670.

[10] R. Smith, "On removing the primary field from fixed-wing time-domain airborne electromagnetic data: Some consequences for quantitative modelling, estimating bird position and detecting perfect conductors," *Geophys. Prospecting*, vol. 49, no. 4, pp. 405–416, Dec. 2001.

[11] B. Gebauer, M. Hanke, A. Kirsch, W. Muniz, and C. Schneider, "A sampling method for detecting buried objects using electromagnetic scattering," *Inverse Problem*, vol. 21, no. 6, p. 2035, Nov. 2005.

[12] G. A. Newman and D. L. Alumbaugh, "Frequency-domain modelling of airborne electromagnetic responses using staggered finite differences1," *Geophys. Prospecting*, vol. 43, no. 8, pp. 1021–1042, Nov. 1995.

[13] Y. Liu, X.-B. Wang, and Y. Wang, "Numerical modeling of the 2D time-domain transient electromagnetic secondary field of the line source of the current excitation," *Appl. Geophys.*, vol. 10, no. 2, pp. 134–144, Jun. 2013.

[14] H. Hu, H. Ye, and Y. Jin, "Fast calculation of scattering in planar uniaxial anisotropic multilayers," *IEEE Access*, vol. 7, pp. 185941–185950, 2019.

[15] A. V. Grayver and M. Bürg, "Robust and scalable 3-D geo-electromagnetic modelling approach using the finite element method," *Geophys. J. Int.*, vol. 198, no. 1, pp. 110–125, 2014.

[16] Y. Zhou, L. Shi, N. Liu, C. Zhu, Y. Sun, and Q. H. Liu, "Mixed spectral-element method for overcoming the low-frequency breakdown problem in subsurface em exploration," *IEEE Trans. Geosci. Remote Sens.*, vol. 55, no. 6, pp. 3488–3500, Jun. 2017.

[17] K. Chen, X. Hou, M. Zhuang, N. Liu, and Q. H. Liu, "An efficient mixed finite-element time-domain method for complex electrically small problems," *IEEE Trans. Microw. Theory Techn.*, vol. 67, no. 4, pp. 1285–1294, Apr. 2019.

[18] R. Hong, K. Chen, X. Hou, Q. Sun, N. Liu, and Q. H. Liu, "Mixed finite element method for full-wave simulation of bioelectromagnetism from dc to microwave frequencies," *IEEE Trans. Biomed. Eng.*, vol. 67, no. 10, pp. 2765–2772, Oct. 2020.

[19] J. Zhuo, F. Han, L. Ye, Z. Yu, and Q. H. Liu, "Simulation of electromagnetic scattering of 3-d inhomogeneous biaxial anisotropic magnetodielectric objects embedded in uniaxial anisotropic media by the mixed-order bcgs-fft method," *IEEE Trans. Microw. Theory Techn.*, vol. 66, no. 8, pp. 3745–3755, Aug. 2018.

[20] J. Zhuo, F. Han, N. Liu, L. Ye, H. Liu, and Q. H. Liu, "Derivation and fast computation of dyadic Green's functions of magnetic vector potential for unbounded uniaxial anisotropic media," *J. Appl. Computat. Electromagn. Soc.*, vol. 32, no. 10, pp. 862–871, Oct. 2017.

[21] G. Palacky, "Resistivity characteristics of geologic targets," *Electromagn. Methods Appl. Geophys.*, vol. 1, pp. 53–129, Jan. 1988.

TINGTING HUANG received the B.S. degree from the Wuhan University of Technology, Wuhan, China, in 2018. She is currently pursuing the M.S. degree with Xiamen University, Xiamen, China.

Her current research interests include computational electromagnetics, with a focus on the fast and efficient methods for geological problems.

MINGWEI ZHUANG received the B.S. degree in applied physics from Shandong Jiaotong University, Jinan, China, in 2011. He is currently pursuing the Ph.D. degree with Xiamen University, Xiamen, China.

From 2016 to 2017, he was a Visiting Student with the Department of Electrical and Computer Engineering, Duke University, Durham, NC, USA. His research interests include numerical methods in acoustic, viscoelastic, and poroelastic waves and imaging.

JIANLIANG ZHUO received the B.S. degree in communication engineering and business administration and the M.S. degree in communication and information system from the University of Electronic Science and Technology of China, Chengdu, China, in 2007 and 2011, respectively, and the Ph.D. degree in physical electronics from Xiamen University, Xiamen, China, in 2018.

Since 2018, he has been a Postdoctoral Fellow with the Postdoctoral Mobile Station of Information and Communication Engineering, Xiamen University. His research interests include fast forward solvers in electromagnetics and inverse scattering methods for microelectronics and RF systems.
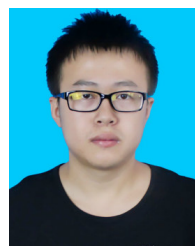
RONGHAN HONG received the B.S. degree in electronics information science and technology from Xiamen University, Xiamen, China, in 2014, where he is currently pursuing the Ph.D. degree with the Department of Electronic Science, Institute of Electromagnetics and Acoustics.

His research interests include electromagnetic forward and inverse scattering problem.

YUEFENG SUN received the Ph.D. degree from Columbia University, New York, NY, USA, in 1994.

He is currently a Mollie B. Ricard A. Williford Professor with the Department of Geology and Geophysics, Texas A&M University, College Station, TX, USA. He has authored numerous articles and patents. His research interests include rock physics, poroelasticity, mechanics and electrodynamics of multiphase fractured porous media, reservoir geophysics, petroleum geology, biogeophysics, and advanced energy research. He is a member of SEG, AAPG, and AGU. He also serves on the Editorial Board of the *Journal of Computational Acoustics*. He is the Director of the TAMU Reservoir Geophysics Program with a research focus on integrating geology, rock physics, geophysics, and reservoir simulation for energy exploration and production.

QING HUO LIU (Fellow, IEEE) received the B.S. and M.S. degrees in physics from Xiamen University, Xiamen, China, and the Ph.D. degree in electrical engineering from the University of Illinois at Urbana-Champaign, Champaign, IL, USA.

From September 1986 to December 1988, he was a Research Assistant with the Electromagnetics Laboratory, University of Illinois at Urbana-Champaign, where he was as a Postdoctoral Research Associate, from January 1989 to February 1990. From 1990 to 1995, he was a Research Scientist and the Program Leader with Schlumberger-Doll Research, Ridgefield, CT, USA. From 1996 to May 1999, he was an Associate Professor with New Mexico State University, Las Cruces, NM, USA. Since June 1999, he has been with Duke University, Durham, NC, USA, where he is currently a Professor of electrical and computer engineering. Since 2005, he has also been the Founder and the Chairman of Wave Computation Technologies, Inc., Durham. His research interests include computational electromagnetics and acoustics, inverse problems, and their application in nanophotonics, geophysics, biomedical imaging, and electronic packaging. He has published widely in these areas.

Dr. Liu is a Fellow of the Acoustical Society of America, the Electromagnetics Academy, and the Optical Society of America. He received the 1996 Presidential Early Career Award for Scientists and Engineers (PECASE) from the White House, the 1996 Early Career Research Award from the Environmental Protection Agency, the 1997 CAREER Award from the National Science Foundation, the 2017 Technical Achievement Award and the 2018 Computational Electromagnetics Award from the Applied Computational Electromagnetics Society, the 2018 Harrington-Mittra Award in Computational Electromagnetics from the IEEE Antennas and Propagation Society, and the University of Illinois from the Urbana-Champaign ECE Distinguished Alumni Award, in 2018. He has served as the Founding Editor-in-Chief for the IEEE JOURNAL ON MULTISCALE AND MULTIPHYSICS COMPUTATIONAL TECHNIQUES. He has served as an IEEE Antennas and Propagation Society Distinguished Lecturer.

• • •